

Energy-Efficient UAV Multicasting with Simultaneous FSO Backhaul and Power Transfer

Yue Ling Che, *Member, IEEE*, Weibin Long, Sheng Luo, *Member, IEEE*, Kaishun Wu, *Member, IEEE*, and Rui Zhang, *Fellow, IEEE*

Abstract—This letter studies an unmanned aerial vehicle (UAV) aided multicasting (MC) system, which is enabled by simultaneous free space optics (FSO) backhaul and power transfer. The UAV applies the power-splitting technique to harvest wireless power and decode backhaul information simultaneously over the FSO link, while at the same time using the harvested power to multicast the backhauled information over the radio frequency (RF) links to multiple ground users (GUs). We derive the UAV's achievable MC rate under the Poisson point process (PPP) based GU distribution. By jointly designing the FSO and RF links and the UAV altitude, we maximize the system-level energy efficiency (EE), which can be equivalently expressed as the ratio of the UAV's MC rate over the optics base station (OBS) transmit power, subject to the UAV's sustainable operation and reliable backhauling constraints. Due to the non-convexity of this problem, we propose suboptimal solutions with low complexity. Numerical results show the close-to-optimal EE performance by properly balancing the power-rate tradeoff between the FSO power and the MC data transmissions.

Index Terms—Unmanned aerial vehicle (UAV) aided multicasting (MC), simultaneous free space optics (FSO) backhaul and power transfer, energy efficiency (EE) maximization.

I. INTRODUCTION

The rapid growth of unmanned aerial vehicles (UAVs) has brought fertile applications in wireless communications [1]. Although appealing, the feasibility of the UAV-aided wireless communications still faces crucial challenges. First, due to the limited battery energy on-board, the UAV's mission time is severely constrained. The technique of solar power harvesting can be adopted to prolong the UAV's battery lifetime, but the intermittent solar energy availability is a practical issue [2]. One the other hand, it is also difficult to establish reliable wireless backhaul links for the UAVs. Due to the presence of strong air-to-ground (A2G) line-of-sight (LoS) links, the conventional radio frequency (RF) based wireless backhaul transmission from the terrestrial base station (BS) to the UAV may suffer severe interference from the co-channel terrestrial transmissions, and vice versa [3].

The technology of free space optics (FSO) transmission is promising to address the above two challenges. Due to the narrow beam with intense energy concentration, the FSO beam is able to deliver high power (of, e.g., hundreds of Watts) to the UAV over a long range [4], [5]. By exploiting the large terahertz unlicensed bandwidth, the FSO link also achieves high-speed data rates, without interfering the UAV's

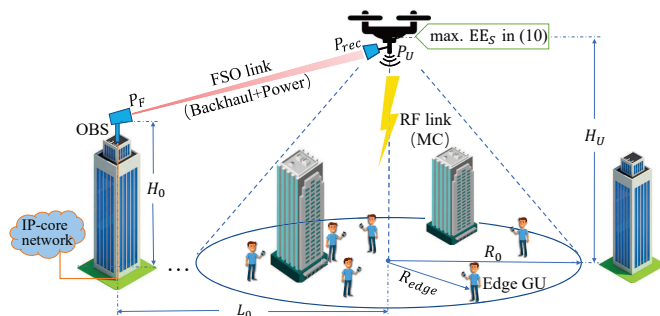


Fig. 1. UAV-aided MC with simultaneous FSO backhaul and power transfer.

RF communication [6]–[8]. Moreover, the simultaneous FSO information and power transfer has been investigated in [9] and [10]. In addition, with the emerging FSO systems developed with fast tracking, the UAV performance loss due to FSO pointing errors can be effectively compensated [11].

In this letter, we propose a novel UAV-aided downlink multicasting (MC) system with simultaneous FSO backhaul and power transfer, as shown in Fig. 1. Adopting the power-splitting based FSO receiver [9], the UAV harvests FSO power and decodes backhaul information simultaneously in the FSO link, while at the same time using the harvested FSO power to multicast the backhauled information to multiple ground users (GUs) in the RF links. Under the homogeneous Poisson point process (PPP) based GU distribution, we derive the UAV's achievable MC rate and the mission completion time using the practical LoS probability-based A2G channel model [12].

To assure the UAV's sustainable and reliable MC over the RF link, an optics base station (OBS) that transmits power and data for charging and backhauling the UAV over the FSO link is essential. We thus aim to maximize the OBS's energy efficiency (EE) at a system level, which is defined as the ratio of the UAV's MC rate over the OBS transmit power, by jointly optimizing the OBS transmit power and the power-splitting ratio for the FSO link, the UAV transmit power for the RF link, and the UAV altitude, subject to the UAV's FSO power harvesting (FPH) and FSO backhauling rate (FBR) constraints. This optimization problem is non-convex, and thus difficult to be solved optimally. Despite of that, we obtain the optimal OBS transmit power and power-splitting ratio in closed-forms under arbitrarily given UAV transmit power and altitude. Then, by proposing a tight approximation to the system EE, we obtain suboptimal UAV transmit power and altitude with low complexity. Numerical results show the close-to-optimal EE performance, which achieves a proper power-rate tradeoff between maximizing the FSO power and the MC data rate.

Y. L. Che, W. Long, S. Luo, and K. Wu are with the College of Computer Science and Software Engineering, Shenzhen University, China (e-mail: yuelingche@szu.edu.cn, 1800271002@email.szu.edu.cn, {sluo,wu}@szu.edu.cn).

R. Zhang is with the Department of Electrical and Computer Engineering, National University of Singapore (e-mail: elezhang@nus.edu.sg).

In the literature, the UAV communications have been studied in [4] and [5] with FSO power transfer, or [6] and [7] with FSO backhauling, respectively. It is noted that only limited works such as [10] and [14] have considered simultaneous FSO backhaul and power transfer enabled UAV communication systems, while they do not address how to efficiently use the UAV's harvested FSO power for optimizing its RF communication performance. To our best knowledge, our proposed energy-efficient UAV MC by jointly designing the UAV's FSO and RF links under practical UAV power consumption and A2G channel models is new and has not been reported in the literature yet.

II. SYSTEM MODEL

As shown in Fig. 1, a set of GUs are distributed following a homogeneous PPP $\Psi(\lambda_G)$ of density $\lambda_G > 0$ within the area of $\phi(\mathbf{o}, R_0)$, where $\phi(\mathbf{o}, R_0)$ represents a circular area of radius R_0 centered at the origin $\mathbf{o} = (0, 0)$ on the horizontal plane. We say GU- i locating at $\mathbf{x}_i \in \Psi(\lambda_G)$ is of radius r if $\|\mathbf{x}_i\| = r$, where $\|\cdot\|$ is the Euclidean norm. The UAV hovers above \mathbf{o} for achieving high-quality RF communication, and is installed with a power-splitting based FSO receiver and an RF transmitter. To avoid transmission blockage, the OBS is deployed at a high altitude (e.g., on top of a building [6]) of H_0 . Denote the UAV's altitude as $H_U \in [H_0, H_{\max}]$, and its horizontal distance to the OBS as $L_0 \geq 0$.

A. Downlink RF Multicasting

Under the LoS-probability based A2G channel in [12] and [13], we use a binary indicator with $\mu(r) = 1$ or $\mu(r) = 0$ to denote the occurrence of LoS or NLoS link from the UAV to a GU at radius r , respectively. The A2G channel $h(r)$ is thus given by

$$h(r) = \begin{cases} (H_U^2 + r^2)^{-\frac{\alpha_L}{2}}, & \text{if } \mu(r) = 1, \\ (H_U^2 + r^2)^{-\frac{\alpha_N}{2}}, & \text{if } \mu(r) = 0, \end{cases} \quad (1)$$

where α_L and α_N with $\alpha_L < \alpha_N$ denote the LoS and NLoS channel path-loss exponents, respectively. We adopt the LoS probability $\mathcal{P}_L(r) \triangleq \mathbb{P}(\mu(r) = 1) = \frac{1}{1 + a \exp(-b(\theta(r) - a))}$, where a and b are environment-related constant parameters, and $\theta(r) = \frac{180}{\pi} \arctan(\frac{H_U}{r})$ is the A2G elevation angle. The NLoS probability is thus obtained as $\mathcal{P}_N(r) = 1 - \mathcal{P}_L(r)$.

Let $P_U \in [0, P_{\max}]$ denote the UAV's transmit power, where P_{\max} is the UAV's maximally allowable transmit power. The GU's received signal-to-noise ratio (SNR) over the LoS or NLoS link is given as $\Gamma_L(r) = \frac{P_U}{\sigma_L^2} (H_U^2 + r^2)^{-\frac{\alpha_L}{2}}$ or $\Gamma_N(r) = \frac{P_U}{\sigma_N^2} (H_U^2 + r^2)^{-\frac{\alpha_N}{2}}$, respectively, where σ_L^2 and σ_N^2 are the GU's received noise power strength in LoS and NLoS link, respectively. Denoting the bandwidth of the RF link as B , the average transmission rate (in bits/s) achieved at a GU at radius $r \in [0, R_0]$ is obtained as

$$\bar{C}(r) = \mathcal{P}_L(r) B \log_2(1 + \Gamma_L(r)) + \mathcal{P}_N(r) B \log_2(1 + \Gamma_N(r)). \quad (2)$$

It is easy to show that a lower bound of $\bar{C}(r)$ is given by

$$\bar{C}_{low}(r) \triangleq \mathcal{P}_L(r) B \log_2(1 + \Gamma_L(r)) \leq \bar{C}(r). \quad (3)$$

As will be shown in Section IV by simulations, for any given $R_0 > 0$ and $r \in [0, R_0]$, since $\mathcal{P}_L(r)$ increases (and thus $\mathcal{P}_N(r)$

decreases) over H_U , which leads to $\mathcal{P}_L(r) > \mathcal{P}_N(r)$ when H_U is large, and also due to $\alpha_L < \alpha_N$ and thus $\Gamma_L > \Gamma_N$ in general, $\bar{C}_{low}(r)$ is generally close to $\bar{C}(r)$, when H_U is sufficiently large so that $H_U \geq H_0$. We hence use $\bar{C}_{low}(r)$ to approximate the more complicated $\bar{C}(r)$ in the following.

Moreover, suppose that the UAV's common information file for downlink MC is of \bar{D} bits. As $\bar{C}_{low}(r)$ decreases over r , the UAV's downlink MC is completed if the edge GU at radius $R_{edge} = \max_{\mathbf{x}_i \in \Psi(\lambda_G)} \|\mathbf{x}_i\|$ receives the complete file of \bar{D} bits. Based on the null-probability of the PPP, the cumulative distribution function (CDF) of R_{edge} is obtained as [15]

$$\begin{aligned} \mathbb{P}(R_{edge} \leq r) &= \mathbb{P}(\text{no GUs exist within } \phi(\mathbf{o}, R_0) - \phi(\mathbf{o}, r)) \\ &= e^{-\pi \lambda_G (R_0^2 - r^2)}, \end{aligned} \quad (4)$$

where the circular ring $\phi(\mathbf{o}, R_0) - \phi(\mathbf{o}, r)$ is of radius between r and R_0 . By differentiating (4) over r , the probability density function (pdf) of R_{edge} is obtained as $f_{R_{edge}}(r) = e^{-\pi \lambda_G (R_0^2 - r^2)} 2\pi \lambda_G r$. The average downlink transmission rate achieved at the edge GU is hence given by

$$\begin{aligned} \bar{C}_{edge} &= \int_{r=0}^{R_0} \bar{C}_{low}(r) f_{R_{edge}}(r) dr \\ &= \int_{r=0}^{R_0} \mathcal{P}_L(r) B \log_2(1 + \Gamma_L(r)) e^{-\pi \lambda_G (R_0^2 - r^2)} 2\pi \lambda_G r dr. \end{aligned} \quad (5)$$

As a result, the average mission completion time for the UAV's downlink MC can be approximated as $T_{MC} = \bar{D} / \bar{C}_{edge}$.

B. Simultaneous FSO Backhaul and Power Transfer

We now consider the FSO transmissions, where the intensity modulation/direct detection (IM/DD) is applied [6]. The OBS-to-UAV distance is obtained as $L_{back} = \sqrt{L_0^2 + (H_U - H_0)^2}$. Let D_r and θ_t denote the diameter of the FSO receiver at the UAV and the full transmitting divergence angle, respectively. From [16], the FSO channel path loss is mainly affected by the following three phenomena: 1) the FSO receiver's responsivity, which is represented by a constant $\tau_e \in (0, 1)$; 2) the atmospheric turbulence induced fading, which is modeled as $\frac{D_r^2}{\theta_t^2 L_{back}^2} 10^{-\kappa \frac{L_{back}}{10}}$ with a weather-dependent coefficient κ ; and 3) the random geometric and misalignment loss (GML), which is caused by the UAV's fluctuations around its hovering location. In this letter, we focus on the average received power strength at the UAV, and use τ_{GML} to represent the average GML for the FSO channel, which can be obtained numerically based on the GML's pdf derived in [16]. As a result, denoting the OBS transmit power as P_F , the average received FSO power at the UAV is expressed as

$$P_{rec} = P_F \omega(H_U) = P_F \tau_e \tau_{GML} \frac{D_r^2}{\theta_t^2 L_{back}^2} 10^{-\kappa L_{back}/10}, \quad (6)$$

where $\omega(H_U) = \frac{\tau_e \tau_{GML} D_r^2}{\theta_t^2 L_{back}^2} 10^{-\kappa \frac{L_{back}}{10}}$ is the average FSO channel power gain.

Next, let $\rho \in [0, 1]$ denote the power-splitting ratio, where $P_{rec}\rho$ amount of power is used to decode backhaul information, and the remaining power of $P_{rec}(1 - \rho)$ is for UAV power harvesting. For the IM/DD FSO channel, the theoretical information capacity remains unknown [17]. However, as validated by the test fields in [6], the achievable FSO throughput at the UAV can be properly expressed as

$$D_{back} = T_{MC} \frac{W}{2} \log_2 \left(1 + \frac{P_F \omega(H_U) \rho}{\sigma_U^2 \beta} \right), \quad (7)$$

where T_{MC} is applied since the UAV operates over the FSO and RF links at the same time, $W > B$ is the FSO channel

bandwidth, σ_U^2 is the UAV's received noise power, and the division by 2 is due to the real-valued Gaussian channel for the IM/DD FSO link. Particularly, the empirical factor β in (7) is introduced to include all the implementation-related SNR losses in practice, which includes, e.g., the reduced modulation current for the IM/DD channel, the non-ideal channel coding, and the FSO pointing errors. It is also noted that when $\beta = \frac{2\pi}{\epsilon}$, D_{back} in (7) becomes the well-known FSO throughput lower-bound in [17], without considering the above mentioned implementation-related SNR losses. We hence assume that $\beta \geq \frac{2\pi}{\epsilon}$ in this letter. This is also in accordance with the empirical value $\beta = 15$ dB obtained in [6]. Since $D_{back} \geq \bar{D} = T_{MC}\bar{C}_{edge}$ is required for reliably backhauling the UAV, the FBR constraint is given as

$$\frac{W}{2} \log_2 \left(1 + \frac{P_F \omega(H_U) \rho}{\sigma_U^2 \beta} \right) \geq \bar{C}_{edge}. \quad (8)$$

Moreover, we consider a linear FPH model based on [4] and [5], where the UAV's harvested FSO power is expressed as $\eta P_{rec}(1-\rho)$ with constant FPH efficiency $\eta \in (0, 1)$. The complicated non-linear FPH efficiency will be studied in our future work. Let P_{hov} denote the UAV's propulsion power for hovering with $P_{hov} \gg P_U$ in practice from [18] and [19]. To assure the UAV's sustainable operation, we obtain the UAV's FPH constraint as follows:

$$\eta P_F \omega(H_U)(1-\rho) \geq P_{hov} + P_U. \quad (9)$$

At last, define the system-level energy efficiency as $EE_S \triangleq \bar{D}/E_{total}$, where $E_{total} = P_F T_{MC}$ is the overall FSO energy consumption for backhauling and charging the UAV over the FSO link, such that the UAV's MC mission over the RF link to deliver \bar{D} bits of common file can be completed within T_{MC}^1 . Since the common information file is completely delivered to all GUs within the corresponding time of $T_{MC} = \bar{D}/\bar{C}_{edge}$, regardless of its size \bar{D} , EE_S can be further expressed as

$$EE_S = \frac{\bar{C}_{edge}}{P_F}. \quad (10)$$

III. SYSTEM-LEVEL EE MAXIMIZATION

In this section, we aim to maximize EE_S in (10), by jointly optimizing the OBS transmit power P_F , the power-splitting ratio ρ , the UAV's altitude H_U and transmit power P_U , subject to the FBR constraint in (8) and the FPH constraint in (9) at the UAV. The optimization problem is formulated as follows.

$$(P1) : \max_{\substack{P_F, \rho, \\ H_U, P_U}} \frac{\bar{C}_{edge}}{P_F} \\ \text{s.t. } 0 \leq \rho \leq 1, 0 \leq P_U \leq P_{\max}, P_F > 0, \\ H_0 \leq H_U \leq H_{\max}, (8), (9).$$

Due to the complicated expression of \bar{C}_{edge} in (5) and coupled decision variables, problem (P1) is non-convex in general. To solve problem (P1) efficiently, in the following, we first obtain the optimal P_F and ρ under any given H_U and P_U , and then derive the optimal H_U and P_U .

First, we optimize P_F and ρ for the FSO link under any given H_U and P_U . In this case, both of the UAV's power consumption $P_U + P_{hov}$ and the MC rate \bar{C}_{edge} over the RF link become fixed. As a result, maximizing $\frac{\bar{C}_{edge}}{P_F}$ in problem

(P1) is equivalent to minimizing P_F over the FSO link subject to (8) and (9), which leads to the following proposition.

Proposition 3.1: Let $Q_I = \frac{\sigma_U^2 \beta}{\omega(H_U)} (2^{\frac{\bar{C}_{edge}}{W}} - 1)$ and $Q_E = \frac{P_U + P_{hov}}{\eta \omega(H_U)}$. For any arbitrarily given $P_U \in [0, P_{\max}]$ and $H_U \in [H_0, H_{\max}]$ at the UAV, the optimal $P_F(P_U, H_U)$ and $\rho(P_U, H_U)$ for the FSO link are obtained in closed-forms as

$$P_F(P_U, H_U) = Q_I + Q_E, \quad \rho(P_U, H_U) = \frac{Q_I}{Q_I + Q_E}. \quad (11)$$

Proposition 3.1 can be shown by noting from (8) and (9) that $Q_I \leq P_F \rho$ and $Q_E \leq P_F(1-\rho)$, respectively, and thus $P_F \geq Q_I + Q_E$, which yields (11) to maximize $\frac{\bar{C}_{edge}}{P_F}$ under a fixed \bar{C}_{edge} . Its proof is thus omitted for brevity.

From (11), both constraints in (8) and (9) hold with equalities under the optimal $P_F(P_U, H_U)$ and $\rho(P_U, H_U)$. Hence, all the UAV's harvested FSO power is consumed completely to support its hovering and simultaneous communication over the RF links for EE maximization.

Next, we consider the RF link. Under the optimal $P_F(P_U, H_U)$ and $\rho(P_U, H_U)$ in Proposition 3.1, problem (P1) is reduced to the following problem:

$$(P2) : \max_{P_U, H_U} EE_U \triangleq \frac{\bar{C}_{edge}}{\frac{\sigma_U^2 \beta}{\omega(H_U)} (2^{\frac{\bar{C}_{edge}}{W}} - 1) + \frac{P_U + P_{hov}}{\eta \omega(H_U)}} \\ \text{s.t. } 0 \leq P_U \leq P_{\max}, H_0 \leq H_U \leq H_{\max}, \quad (12)$$

where EE_U is obtained by substituting (11) into (10). (P2) is non-convex due to the fractional form of the objective with complicated \bar{C}_{edge} . To deal with the complicated \bar{C}_{edge} , an upper-bound of \bar{C}_{edge} is proposed as follows.

Proposition 3.2: Define $\bar{C}_{edge}^{upp} \triangleq \mu B \log_2(1 + P_U y(H_U))$, where $\mu = \int_{r=0}^{R_0} \mathcal{P}_L(r) e^{-\pi \lambda_G (R_0^2 - r^2)} 2\pi \lambda_G r dr$ and $y(H_U) = \frac{1}{\sigma_U^2} \int_{r=0}^{R_0} \frac{1}{\mu} \mathcal{P}_L(r) (H_U^2 + r^2)^{-\frac{\alpha}{2}} e^{-\pi \lambda_G (R_0^2 - r^2)} 2\pi \lambda_G r dr$. When $H_U > \sqrt{\alpha_L + 1} R_0$, $\bar{C}_{edge} \leq \bar{C}_{edge}^{upp}$ holds.

Proof: Please refer to Appendix A. ■

By replacing \bar{C}_{edge} in (12) with \bar{C}_{edge}^{upp} , problem (P2) is transformed into the following problem.

$$(P3) : \max_{P_U, H_U} \widetilde{EE}_U \triangleq \frac{\bar{C}_{edge}^{upp}}{\frac{\sigma_U^2 \beta}{\omega(H_U)} (2^{\frac{\bar{C}_{edge}^{upp}}{W}} - 1) + \frac{P_U + P_{hov}}{\eta \omega(H_U)}} \\ = \frac{(\sigma_U^2 \beta)^{-1} \mu B \omega(H_U) \log_2(1 + P_U y(H_U))}{(1 + P_U y(H_U))^{\frac{2\mu B}{W}} + \frac{P_U + P_{hov}}{\eta \sigma_U^2 \beta} - 1} \\ \text{s.t. } 0 \leq P_U \leq P_{\max}, H_0 \leq H_U \leq H_{\max}. \quad (13)$$

It is observed that EE_U in (12) and \widetilde{EE}_U in (13) are of the same fractional structure with a practically large P_{hov} in the denominator, while the numerator and denominator both increase over \bar{C}_{edge} or \bar{C}_{edge}^{upp} . It is thus easy to verify that both EE_U and \widetilde{EE}_U are more dominated by the large P_{hov} than the corresponding edge GU rates. As a result, although $\bar{C}_{edge} \leq \bar{C}_{edge}^{upp}$ holds under a large H_U , as will be shown in Section IV by simulations, \widetilde{EE}_U is generally a tight approximation to EE_U regardless of H_U 's values, under the optimal P_U to problem (P3) and (P2), respectively.

From (14) under \bar{C}_{edge}^{upp} 's expression, although \widetilde{EE}_U is neither convex nor concave over (P_U, H_U) , the optimal $P_U(H_U)$ at any given H_U to problem (P3) is obtained as follows.

¹To focus on the joint design of the FSO and RF links, the OBS's and GUs's circuit energy consumptions are not considered.

Proposition 3.3: For any given H_U , let $g(P_U) \triangleq \frac{\partial \widetilde{\text{EE}}_U}{\partial P_U}$. The optimal $\widetilde{P}_U(H_U)$ to problem (P3) is obtained as

$$P_U(H_U) = \begin{cases} P_{\max}, & \text{if } g(P_{\max}) > 0, \\ P_s, & \text{otherwise,} \end{cases} \quad (15)$$

where $P_U = P_s$ is the unique solution to $g(P_U) = 0$ when $g(P_{\max}) \leq 0$.

Proof to Proposition 3.3 is obtained by showing that $g(P_U) > 0$ at $P_U = 0$ and $g(P_U)$ monotonically decreases over P_U since $\frac{dg(P_U)}{dP_U} < 0$, which leads to the conclusion that $\widetilde{\text{EE}}_U$ increases over $P_U \in [0, P_{\max}]$ if $g(P_{\max}) > 0$, or otherwise, $\widetilde{\text{EE}}_U$ first increases and then decreases over P_U , and thus (15) follows, while the details are omitted for brevity.

By substituting (15) into (14), the optimal H_U^{EE} and thus $P_U^{EE} = P_U(H_U^{EE})$ to problem (P3) are then easily obtained via one-dimensional exhaustive search over $H_U \in [H_0, H_{\max}]$. Hence, given a quantization step size $\delta > 0$, the complexity for solving (P3) is only of $\mathcal{O}(N)$, where $N = \lfloor \frac{H_{\max} - H_0}{\delta} \rfloor$ and $\lfloor x \rfloor$ denotes the floor operation of $x \in \mathbb{R}$.

Finally, as detailed in Algorithm 1, by adopting the optimal H_U^{EE} and P_U^{EE} to problem (P3) as suboptimal solutions to problem (P2), the original problem (P1) is solved with suboptimal P_U^{EE} , H_U^{EE} , P_F^{EE} , and ρ^{EE} , where P_F^{EE} and ρ^{EE} are obtained by substituting P_U^{EE} and H_U^{EE} into (11).

Algorithm 1 Proposed algorithm for solving problem (P1).

- 1: initialize δ and $\text{EE}_{\max} = 0$.
 - 2: **for** each $H_U \in \{H_0, H_0 + \delta, \dots, H_0 + N\delta\}$ **do**
 - 3: set $\widetilde{P}_U(H_U)$ as in (15) and $\widetilde{\text{EE}}_U$ as in (14);
 - 4: **if** $\widetilde{\text{EE}}_U > \text{EE}_{\max}$ **then**
 - 5: set $\text{EE}_{\max} = \widetilde{\text{EE}}_U$, $H_U^{EE} = H_U$, $P_U^{EE} = \widetilde{P}_U(H_U)$;
 - 6: **end if**
 - 7: **end for**
 - 8: set P_F^{EE} and ρ^{EE} as in (11) using P_U^{EE} and H_U^{EE} ;
 - 9: return P_U^{EE} , H_U^{EE} , P_F^{EE} , and ρ^{EE} .
-

Thanks to the closed-form expressions in (11), the complexity of Algorithm 1 is also of $\mathcal{O}(N)$ only, which equals that for solving problem (P3). Therefore, problem (P1) is efficiently solved by our proposed Algorithm 1 with low complexity.

IV. NUMERICAL RESULTS

This section provides numerical results to validate our analysis and evaluate the proposed solution. We consider $\beta = 15$ dB, $\kappa = 4.3 \times 10^{-4}/\text{m}$, $\theta_t = 0.06$ rads, $D_t = 0.2$ m, $\eta = 0.2$, and $\tau_e \tau_{GML} = 0.9$ based on [6] and [11]. Unless specified otherwise, we set $H_{\max} = 200$, $L_0 = 150$, $R_0 = 50$, all in meters, $\alpha_L = 3$, $\alpha_N = 5$, $\sigma_L^2 = \sigma_U^2 = 10^{-6}$ mW, $\sigma_N^2 = 0.8 \times 10^{-6}$ mW, $\delta = 1$, $P_{\max} = 200$ mW, and $P_{\text{hov}} = 1$ KW as in [18].

First, we validate that $\widetilde{C}_{\text{low}}(r)$ in (3) is close to $\widetilde{C}(r)$ in (2) when H_U is sufficiently large, under the typical environment of Dense Urban or High-rise Urban in [12] with generally low LoS probabilities. For each environment, we conduct a worst-case study by focusing on a GU at radius R_0 , which has the lowest LoS probability and thus the largest rate gap $\widetilde{C}(r) - \widetilde{C}_{\text{low}}(r)$ among all $r \in [0, R_0]$ for any given H_U . From Fig. 2, it is first observed that $\widetilde{C}(R_0)$ in the Dense Urban case is always higher than that in the High-rise Urban case,

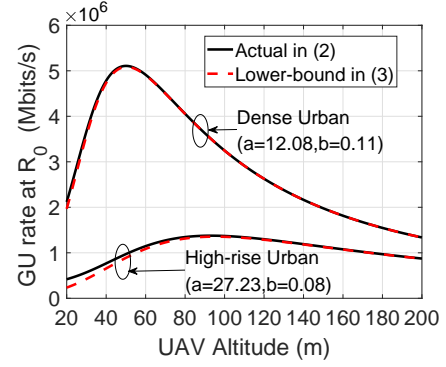
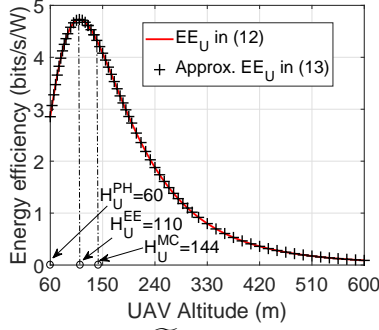
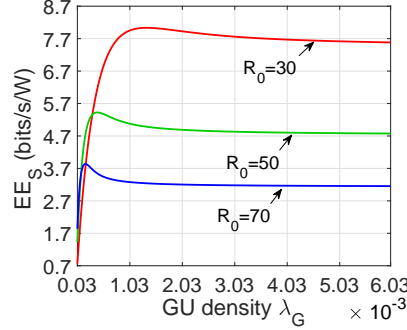
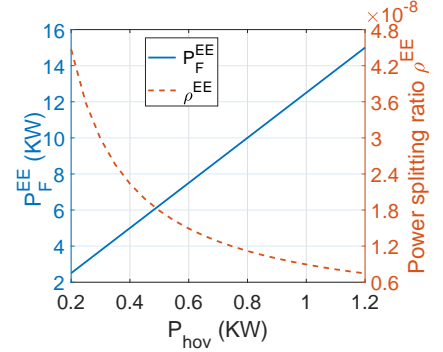


Fig. 2. $\widetilde{C}(R_0)$ and its lower-bound $\widetilde{C}_{\text{low}}(R_0)$ over H_U .

due to the larger LoS probability in the former case. It is also observed that with $B = 20$ MHz, the lower bound $\widetilde{C}_{\text{low}}(R_0)$ is always tight to the actual $\widetilde{C}(R_0)$ in the Dense Urban case. In the High-rise Urban case, although the rate gap is relatively larger when H_U is small, as the LoS probability increases over H_U , the rate gap becomes trivial when H_U is sufficiently large. For example, when $H_U \geq 60$ m, the normalized rate gap with $\frac{\widetilde{C}(R_0) - \widetilde{C}_{\text{low}}(R_0)}{\widetilde{C}(R_0)} \leq 0.052$ is obtained for the considered worst case. For all simulations in the following, we consider the High-rise Urban environment and set $H_0 = 60$ m.

Next, we validate that $\widetilde{\text{EE}}_U$ in (13) is a good approximation to EE_U in (12) in Fig. 3. We set $H_{\max} = 600$ m. It is first found that at each value of H_U , the optimal P_U that maximizes EE_U with $\widetilde{C}_{\text{edge}}^{\text{upp}}$ or EE_U with $\widetilde{C}_{\text{edge}}$, which is obtained based on (15) or via one-dimensional search, is equal to P_{\max} . Under the optimal P_{\max} , it is then observed that, as analyzed in Section III, due to the dominance of the large P_{hov} , $\widetilde{\text{EE}}_U$ is only trivially larger than EE_U at each H_U , where the resultant EE gap is $\widetilde{\text{EE}}_U - \text{EE}_U = 9.1172 \times 10^{-7}$ at its largest value over all H_U 's. It is further observed that as H_U increases, both EE_U and $\widetilde{\text{EE}}_U$ first increase due to the increased LoS probability, and then decrease after achieving their respective maximum due to the significantly decreased $\omega(H_U)$. In addition, let H_U^{PH} and H_U^{MC} denote the UAV's altitudes that maximize P_{rec} in (6) and $\widetilde{C}_{\text{edge}}$ in (5), respectively. It is observed that $H_U^{PH} < H_U^{EE} < H_U^{MC}$. Therefore, the proposed H_U^{EE} for EE maximization strikes a proper balance between FSO power and MC rate maximizations.

Fig. 4 shows EE_S in (10) over the GU density λ_G by applying Algorithm 1. For each value of R_0 , it is observed that EE_S increases when λ_G , where $\widetilde{C}_{\text{edge}}$ in (5) increases fast, and after achieving its maximum value (at, e.g., $\lambda_G = 1.23 \times 10^{-3}$ when $R_0 = 30$), EE_S begins to decrease over λ_G , due to the resultant increasing of R_{edge} and thus H_U^{EE} to enhance the LoS probability, which in turn leads to dominantly increased OBS transmit power P_F over $\widetilde{C}_{\text{edge}}$ to meet (9). Moreover, when λ_G is sufficiently large such that R_{edge} equals R_0 with probability close to 1, H_U^{EE} does not increase any more and thus EE_S becomes a constant in Fig. 4. Similarly, when λ_G is very small, EE_S is dominated by the increasing of $\widetilde{C}_{\text{edge}}$ and thus increases over R_0 ; and when λ_G is large, EE_S is dominated by the increasing of P_F and thus generally decreases over R_0 . In addition, it is also observed from Fig. 4

Fig. 3. EE_U and \widetilde{EE}_U over H_U .Fig. 4. System-level EE over λ_G .Fig. 5. P_F^{EE} and ρ^{EE} over P_{hov} .

that the optimal GU density that maximizes EE_S increases as R_0 decreases. This is due to the increased \widetilde{C}_{edge} in (5) under a smaller R_0 , which allows the UAV to serve more GUs at a lower altitude H_U^{EE} using a smaller P_F under (8) and (9).

Finally, Fig. 5 shows P_F^{EE} and ρ^{EE} over P_{hov} , where $P_U^{EE} = P_{max}$ at each P_{hov} . Since $P_{hov} \gg P_U^{EE}$ in practice, the UAV's harvested FSO power is mainly used to satisfy P_{hov} . This explains the generally low EE_S in Figs. 3 and 4, which further shows the importance of system-level EE design for FSO-powered UAV communications. Although ρ^{EE} is very small, due to the large P_F^{EE} , the achieved SNR at the UAV is still acceptable with, e.g., $\frac{P_F \omega(H_U) \rho}{\sigma_U^2 \beta} = 1.42$ in (7) when $P_{hov} = 1$ KW.

V. CONCLUSION

This letter proposed a sustainable and reliable UAV MC system enabled by simultaneous FSO backhaul and power transfer. We investigated the important system-level EE maximization design by jointly optimizing the FSO and RF transmissions and the UAV altitude. Despite of the non-convexity of the proposed problem, we obtained close-to-optimal solutions with low complexity by tightly approximating the complicated EE. It was shown that the proposed design can properly balance the FSO power transfer and the RF downlink MC. It is our hope that this work can provide design insights on the FSO-based sustainable and reliable UAV RF access network. It is also an interesting future direction to extend this work to mobile UAV scenarios by invoking UAV trajectory design to further improve the EE for FSO-enabled UAV communications.

APPENDIX A PROOF TO PROPOSITION 3.2

When $H_U > \sqrt{\alpha_L + 1}R_0$, since $(H_U^2 + r^2)^{-\frac{\alpha_L}{2}}$ is concave over r with $\frac{\partial^2}{\partial r^2}(H_U^2 + r^2)^{-\frac{\alpha_L}{2}} < 0$, and the concave function $\log_2(1 + \frac{P_U}{\sigma_L^2}X)$ monotonically increases over $X > 0$, we obtain that $Z(r) \triangleq \log_2[1 + \frac{P_U}{\sigma_L^2}(H_U^2 + r^2)^{-\frac{\alpha_L}{2}}]$ is concave over $r > 0$. Then, defining a pdf of $r \in [0, R_0]$ as $f'(r) = \frac{1}{\mu} \mathcal{P}_L(r) f_{R_{edge}}(r)$ with $\int_0^{R_0} f'(r) dr = 1$, we obtain from (5) that $\widetilde{C}_{edge} = \mu B \int_0^{R_0} f'(r) Z(r) dr \leq C_{edge}^{upp}$, by applying Jensen's inequality with the concave $Z(r)$. Proposition 3.2 thus follows.

REFERENCES

- [1] Y. Zeng, Q. Wu, and R. Zhang, "Accessing from the sky: A tutorial on UAV communications for 5G and beyond," *Proc. IEEE*, vol. 107, no. 12, pp. 2327-2375, Dec. 2019.
- [2] Y. Sun *et al.*, "Optimal 3D-trajectory design and resource allocation for solar-powered UAV communication systems," *IEEE Trans. Commun.*, vol. 67, no. 6, pp. 4281-4298, Jun. 2019.
- [3] C. Qiu *et al.*, "Multiple UAV-mounted base station placement and user association with joint fronthaul and backhaul optimization," *IEEE Trans. Commun.*, vol. 68, no. 9, pp. 5864-5877, Sep. 2020.
- [4] J. Ouyang, Y. L. Che, J. Xu, and K. Wu, "Throughput maximization for laser-powered UAV wireless communication systems," in *Proc. IEEE Int. Conf. Commun. Workshops (ICC Workshops)*, May 2018, pp. 1-6.
- [5] M. M. Zhao, Q. Shi, and M. J. Zhao "Efficiency maximization for UAV-enabled mobile relaying systems with laser charging," *IEEE Trans. Wireless Commun.*, vol. 19, no. 5, pp. 3257-3272, May, 2020.
- [6] D. Schulz *et al.* "Robust optical wireless link for the backhaul and fronthaul of small radio cells," *J. Lightw. Technol.*, vol. 34, no. 6, pp. 1523-1532, Mar. 15, 2016.
- [7] H. Ajam *et al.*, "Ergodic sum rate analysis of UAV-based relay networks with mixed RF-FSO channels," *IEEE Open J. Commun. Soc.*, vol. 1, pp. 164-178, Jan. 2020.
- [8] Y. Wang *et al.*, "Deep learning for optimal deployment of UAVs with visible light communications," *IEEE Trans. Wireless Commun.*, vol. 19, no. 11, pp. 7049-7063, Nov. 2020.
- [9] Z. Wang *et al.*, "On the design of a solar-panel receiver for optical wireless communications with simultaneous energy harvesting," *IEEE J. Sel. Areas Commun.*, vol. 33, no. 8, pp. 1612-1623, Aug. 2015.
- [10] M.-A. Lahmeri, M. A. Kishk, and M.-S. Alouini, "Stochastic geometry-based analysis of airborne base stations with laser-powered UAVs," *IEEE Commun. Letters*, vol. 24, no. 1, pp. 173-177, Jan. 2020.
- [11] S. V. Kartalopoulos, *Free-Space Optical Networks for Ultra-broad Band Services*. John Wiley and Sons, New Jersey, USA, Aug. 2011.
- [12] A. Al-Hourani, S. Kandeepan, and S. Lardner, "Optimal LAP altitude for maximum coverage," *IEEE Commun. Letters*, vol. 4, no. 6, pp. 569-572, Dec. 2014.
- [13] M. Tatar Mamaghani and Y. Hong, "On the performance of low-altitude UAV-enabled secure af relaying with cooperative jamming and swipt," *IEEE Access*, vol. 7, pp. 153060-153073, 2019.
- [14] P. D. Diamantoulakis *et al.*, "Airborne radio access networks with simultaneous lightwave information and power transfer (SLIPT)," in *Proc. IEEE Global Commun. Conf. (GLOBECOM)*, Dec. 2018, pp. 1-6.
- [15] Y. L. Che, L. Duan, and R. Zhang, "Spatial throughput maximization in large scale wireless powered communication networks," *IEEE J. Sel. Areas Commun.*, vol. 33, no. 8, pp. 1534-1548, Aug. 2015.
- [16] M. Najafi *et al.*, "Statistical modeling of the FSO fronthaul channel for UAV-based communications," *IEEE Trans. Commun.*, vol. 68, no. 6, pp. 3720-3736, Jun. 2020.
- [17] A. Lapidith, S. M. Moser, and M. A. Wigger, "On the capacity of free-space optical intensity channels," *IEEE Trans. Inf. Theory*, vol. 55, no. 10, pp. 4449-4461, Oct. 2009.
- [18] Y. L. Che *et al.*, "UAV-aided information and energy transmissions for cognitive and sustainable 5G networks," *IEEE Trans. Wireless Commun.*, vol. 20, no. 3, pp. 1668-1683, Mar. 2021.
- [19] Z. Yang, W. Xu, and M. Shikh-Bahaei, "Energy efficient UAV communication with energy harvesting," *IEEE Trans. Veh. Technol.*, vol. 69, no. 2, pp. 1913-1927, Feb. 2020.